



1 Performance Evaluation for Retrieving Aerosol Optical Depth from 2 Directional Polarimetric Camera (DPC) based on GRASP Algorithm

3
 4 Shikuan Jin ¹, Yingying Ma ^{1,2,*}, Cheng Chen ⁴, Oleg Dubovik ⁵, Jin Hong ⁶, Boming Liu ¹, Wei
 5 Gong ^{2,3}
 6

7 ¹ State Key Laboratory of Information Engineering in Surveying, Mapping and Remote Sensing,
 8 Wuhan University, China.

9 ² Collaborative Innovation Center for Geospatial Technology, Wuhan 430079, China.

10 ³ School of Electronic Information, Wuhan University, China.

11 ⁴ GRASP-SAS, Remote Sensing Developments, Cite Scientifique, University of Lille, 59655
 12 Villeneuve d'Ascq, France.

13 ⁵ Univ. Lille, CNRS, UMR 8518 - LOA - Laboratoire d'Optique Atmosphérique, Lille, France.

14 ⁶ Anhui Institute of Optics and Fine Mechanics, Chinese Academy of Sciences, Hefei 230031,
 15 China.

16
 17 Corresponding Author: Yingying Ma (yym863@whu.edu.cn)

18 Abstract

19 Aerosol spatial distribution obtained from the satellite sensor is a critical point to understand
 20 regional aerosol environment, anthropogenic aerosol emissions, and global climate change. In this
 21 study, the performance of aerosol optical depth (AOD) retrieval from the Directional Polarimetric
 22 Camera (DPC)/GaoFen-5 by using the Generalized Retrieval of Atmosphere and Surface Properties
 23 (GRASP) algorithm was evaluated on a global basis for the first time. The results showed that the
 24 DPC GRASP/Model scheme, which used several aerosol-type mixings, achieved good performance.
 25 By compared with AERONET observations, the correlation coefficient (R), normalized mean square
 26 error, and Expect Error (EE%) were 0.8982, 0.1008, and 83.16%, respectively. The scattering angle,
 27 number of averaged pixels in retrieval units, and radiative and polarized fitting residuals showed
 28 impacts on the results of AOD retrieval in the DPC GRASP/Model. From the most of AERONET
 29 sites, the R and EE% were larger than ~0.9 and ~80%. Compared with MODIS products, the spatial
 30 and temporal variations of AOD could be caught by the DPC observations with the GRASP/Model,
 31 and compared with the MODIS Dark Target algorithm, the DPC GRASP/Model AOD also showed
 32 a good performance. The above findings validated the ability of DPC sensor to monitor aerosols. It
 33 would contribute to the development of aerosol parameter retrieval from multi-angular polarized
 34 sensors in the future.

35
 36 **Key Words:** GRASP/Model, Aerosol Optical Depth, Directional Polarimetric Camera, GaoFen-5,
 37 Aerosol Parameter Retrieval
 38



39 1. Introduction

40 Aerosol is one of the most important components in the atmosphere. They influence the global
 41 radiation budget ~~balance~~ and climate directly by scattering and absorbing incoming solar radiation
 42 and indirectly by changing cloud microphysical properties (Albrecht 1989; D'Almeida et al. 1991;
 43 Rosenfeld et al. 2008). Due to the different emission sources and relatively transitory lifecycle in
 44 the atmosphere, aerosol particles show large spatiotemporal variability, and ~~it is~~ difficult to describe
 45 uniformly at a global scale (Eck et al. 2010; Jin et al. 2019; Ma et al. 2021). This property can further
 46 affect ~~the~~ atmospheric motion, ~~hydrological~~ cycle, and probably contribute ~~regional~~ extreme
 47 weather events (Nakajima et al. 2007; Guo et al. 2016; Li et al. 2016; Shi et al. 2021). Therefore,
 48 the development of aerosol measurement technologies has ~~been a topic~~ received widely attention in
 49 recent decades.

50 Satellite observation is the ~~mainly~~ approach to monitor and quantify aerosol distributions at a
 51 global scale (Kaufman et al. 1997). Traditional Satellite technology relies on ~~unique channel design~~
 52 ~~and~~ prior assumptions about the properties of the surface and atmosphere, because the prerequisite
 53 for successful retrieval of aerosol is that the aerosol signal should be isolated from a total mixture
 54 of information received by satellite, which includes the combined effect from molecule, aerosol,
 55 cloud, and the underlying surface (Lenoble et al. 2013). For instance, the appropriate spatial
 56 resolution helps to observe aerosol through clear holes in otherwise cloudy skies (Jin et al. 2021).
 57 The choice of spectral channel and bandwidth can avoid impact by gas absorption, ~~if they are~~ in
 58 narrow spectral bands ~~of~~ atmosphere window regions. ~~In addition~~, more importantly, the spectral
 59 channel should be set in a carefully selected band to avoid introducing uncertainty from underlying
 60 surface features ~~in the meantime~~, such as vegetation, bright desert, and ocean color (McCormick et
 61 al. 1979; Rao et al. 1989; Hsu et al. 2004). Based on these principles, a series of aerosol products
 62 from different sensors ~~has~~ been released, and they greatly promote the developments of studies in
 63 aerosol-related fields, including aerosol climate effect, interaction of aerosol and cloud, air quality
 64 and public health, and global climate modeling (Tegen and Lacis 1996; Sayer et al. 2013; Gao et al.
 65 2017; Zhang et al. 2021).

66 With the progress of satellite technology, sensors with broader spectral range, multiple angles,
 67 and polarization observations have ~~also~~ been applied to aerosol observations. ~~The~~ POLDER-3 is the
 68 third sensor in the POLarization and Directionality of the Earth's Reflectance series, carried on the
 69 Polarization and Anisotropy of Reflectances for Atmospheric Science coupled with Observations
 70 from a Lidar (PARASOL), which was launched on December 18, 2004, as part of the A-Train (Tanre
 71 et al. 2011). This instrument views ($\pm 51^\circ$ along track and $\pm 43^\circ$ across track) Earth from ~ 13 different
 72 angles by using a set of wide-field telecentric optics and a rotating filter wheel in nine spectral
 73 channels from 443 to 1020 nm (Deschamps et al. 1994). Among them, three channels in 490, 670,
 74 and 865 nm have polarization observation capabilities. ~~The~~ POLDER-3 provides the longest multi-
 75 angle polarimetric observation record of the Earth-atmosphere system in space to date and the
 76 PARASOL mission was terminated in December 2013 due to limited on-board fuel ~~budget~~. The
 77 Directional Polarimetric Camera (DPC) is the first Chinese multi-angle polarized ~~earth~~ observation
 78 satellite sensor, onboard the fifth satellite (GaoFen-5) of the Chinese High-resolution Earth
 79 Observation Program (Li et al. 2018). It was launched successfully on May 9, 2018, with the
 80 purposes of measuring aerosol parameters and providing information for the assessment of urban
 81 air pollution. The design of DPC is similar to the POLDER-3. It is equipped ~~five~~ non-polarized



bands at 443, 565, 763, 765, and 910 nm and three polarized bands at 490, 670, and 865 nm, with relatively higher spatial resolution of 3.3 km, that can observe Earth from ~9 different angles. Therefore, the DPC occupies an important position in the development of polarization instruments in China, and is expected to provide beneficial information for atmospheric aerosol monitoring and satellite payload research.

The multi-angular polarized sensor can provide much more observations for the same pixel in aerosol parameter retrieval. Compared to traditional spectral measurement, the multi-angle can help constrain bidirectional reflections function, reducing uncertainty from the surface (Diner et al. 1998), while the polarized signal is mainly from atmospheric aerosol and sensitive to particle microphysical properties (Mishchenko and Travis 1997). Generally, the polarized signal can be considered as an independent source of information. A well-known advantage is that the polarized light from the surface is accounts for a small part of the total polarized light compared with that from the particles and shows a feature of almost wavelength independence. In the algorithms for POLDER, the polarized signals at 670 and 865 nm are used for deriving the best aerosol model over the ocean and retrieving Aerosol Optical Depth (AOD) over land, due to the sensitivity to fine particles (Nadal and Bréon 1999; Deuzé et al. 2001; Kacenelenbogen et al. 2006; Ge et al. 2020). In addition, the existence of the cloudbow effect in polarized signal can also be used to recognize cloud mask and detect cloud structure (Breon and Goloub 1998; Breon and Colzy 1999; Li et al. 2021).

However, the algorithms that retrieve aerosol parameters from only one or two polarized channels are still difficult to obtain complex aerosol optical and microphysical parameters, such as aerosol size distribution and absorbing and scattering properties. To solve this problem, the Generalized Retrieval of Atmosphere and Surface Properties (GRASP) algorithm is developed, which provides a novel statistical optimized strategy that allows all aerosol-related measurement data from multi-angular polarized sensors to participate in the retrieval (Dubovik et al. 2014). It points out that the measured redundancy provided by multi-angular polarized sensor is considered to be positive and useful, especially when the observations are larger than the unknowns (Dubovik et al. 2011). At present, the GRASP algorithm has been successfully applied to a variety of sensors to retrieve complex aerosol parameters, including POLDER, lidar, and sun photometer (Li et al. 2019; Chen et al. 2020; Lopatin et al. 2021). In this study, we retrieved AOD from DPC observations by using GRASP algorithm and evaluated possible error influencing factors. At the same time, by comparing MODIS and AERONET observations, the aerosol monitoring performance of DPC were verified in different space and time scales. This will partially lay the foundation for the retrieval of aerosol parameters from multi-angular polarized sensors in the future of China.

2. Satellite and Ground-based Data

2.1 DPC Data

The DPC is a multi-angular polarized sensor carried on the GF-5 satellite, which was launched in May 9, 2018. This sensor completes a scan of entire Earth's surface about every two days at a sun-synchronous orbit and provides a swath of 1850 km with a spatial resolution of 3.3 km (Li et al. 2018). The DPC contains eight bands from 443 to 910 nm with a bandwidth of 10-40 nm that can observe earth from ~9 different angles in a local time of ~13:30 PM. Except for water vapor band (910 nm) and pressure bands (Oxygen A band: 763 and 765 nm), other five bands (443, 490,





565, 670, and 865 nm) are designed for observing aerosol (Li et al. 2018). The polarimetric capability at 490, 670, and 865 nm is realized by a polarized filter wheel (0°, 60°, and 120°) and a step motor (Hagolle et al. 1999). The laboratory calibration uncertainties are ~~relatively~~ 5% for normalized radiation and ~~absolutely~~ 0.02 for Degree Of Linear Polarization (DOLP) (Li et al. 2021). An in-flight calibration study showed that the radiometric calibration error increased to ~9% at 865 nm and the polarimetric calibration **error increase** to ~0.04 at 490 and 670 nm after launch, by respectively applying Rayleigh and glint scenes over ocean (Qie et al. 2021). ~~While~~, degradation of instrument performance over time may result in higher negative radiometric shift (Zhu et al. 2022). Thus, additional correction coefficients were also applied in this study to correct the image of the DPC observations from March to April, 2020. For preparing to retrieve AOD, the processing of DPC data is described in Section 3.2 in detail.

2.2 MODIS aerosol products

The Moderate-resolution Imaging Spectroradiometer (MODIS) has been in service for over two decades, providing valuable **data for the** earth's observations. The MODIS Level 2 C6.1 aerosol product (MxD04) is generated by using Dark Target (DT) algorithm and Deep Blue (DB) algorithm (Hsu et al. 2013; Levy et al. 2013). It provides multi-wavelength AOD data from each individual image with spatial resolutions of 3 km and 10 km. ~~While~~, the MODIS Level 2 C6 aerosol product (MCD19A2) considers temporal and spatial correlation of aerosols, calculating aerosol parameters by using the Multi-Angle Implementation of Atmospheric Cor^{rection} (MAIAC) algorithm from the continuous scenes of two satellites (Terra and Aqua), with a spatial resolution of 1 km (Lyapustin et al. 2018). Compared to global coverage of DT algorithm, the DB algorithm is only applied over land, and the MAIAC algorithm is used over land and part of the surrounding ocean. These MODIS aerosol products have been rigorously tested and verified, and are widely used in aerosol-related studies (Sayer et al. 2014; Che et al. 2019; Zhdanova et al. 2020). Only MODIS data with the highest quality were used in this study.

2.3 AERONET observations

The AErosol RObotic NETwork (AERO^{ENT}) is a federation of ground-based remote sensing aerosol networks, established and expanded by various institutions from different countries (Holben et al. 1998). It has contributed continuous and long-term aerosol optical, microphysical, and radiative properties for more than 25 years in major ecosystems and human activity areas around the world. The AOD data used for validation were acquired from Level 1.5 and Level 2.0 AERONET products, which have been cloud-screened and quality controlled. The uncertainties of AOD are less than 0.02 (Eck et al. 1999). In order to match the AERONET data to the satellite observations, a common approach is followed to averages satellite data within ±30 min and a circle of 0.25° (~25 km) radius centered at the selected site (Sayer et al. 2013). The relationship between multi-wavelength AOD proposed by Ångström (1964) was applied to calculate the AOD at corresponding wavelength of satellite bands from AERONET data.

3. Methods

3.1 Introduction of GRASP algorithm



GRASP is an open-source software package (<https://www.grasp-open.com/>) for calculating and retrieving various optical and microphysical properties of aerosol and surface from observations of different remote sensing instruments, such as satellite, lidar, radiometer, and radiosonde (Dubovik et al. 2021). It was originally designed ~~to improve and~~ solve the problem of aerosol retrieval under high surface reflectance conditions from the PARASOL observations (Dubovik et al. 2014), while now has become a scientifically rigorous and versatile algorithm based on generalization principles that works with diverse remote sensing applications in the community after continuous development (Dubovik et al. 2021). The GRASP algorithm contains two pivotal and independent modules. One is used to calculate the scattering, absorbing, and extinction of light between different media from the physical level, simulating theoretical observational radiation signal, called “Forward Model”. It allows **define** various complex aerosol (size distribution, refractive index, and sphere fraction, etc.) and surface properties (Bidirectional Reflectance/ Polarization Distribution Function, BR/PDF, etc.) in the construction of model. Therefore, this makes it possible to transform from optical observations to aerosol microphysical properties and estimate the surface parameters ~~in the meantime~~ (Dubovik et al. 2011). The other module can be thought of as general mathematical operations without any particularly physical nature, called “Numerical Inversion”. It follows the statistically optimized strategy to fit observations under the fundamental frameworks of the Maximum Likelihood Method and multi-term Least Square Method (Dubovik and King 2000). **By introducing** Lagrange multiplier method, the GRASP also realizes multiple-pixel retrieval, which constrains the variability of aerosol and surface optical properties in fitting process by an extra prior knowledge. Due to the consideration of the surrounding pixel information, the multi-pixel retrieval is more stable, and more importantly, it can make up for the lack of aerosol reflection information in some cases, such as conditions that the signal from aerosol is much less than that from the surface (Dubovik et al. 2011). Based on the above advantages, the GRASP supports input measurements/parameters from different sources and levels, such as normalized and polarized radiance, vertical extinction and backscatter profile, and optical depth. This avoids that the traditional look-up table-based methods are difficult to apply to each other, due to the limitations of different sensor channel and characteristic.

3.2 Pre-processing of DPC Data

In order to partially offset the signal attenuation due to ~~possible~~ instrument aging, before the pre-processing and retrieval, the radiance signals from the DPC were transferred and corrected to normalized radiative and polarized reflectance at top of the atmosphere.

$$[I_N, Q_N, U_N]^T = \pi \cdot [I, Q, U]^T / [E_0 \cdot A'_k(\theta_0) \cdot P'_k(\theta)] \quad (1)$$

where, the $[I, Q, U]^T$ ~~are~~ represent the radiative and polarized radiances, received by the DPC, in the form of the first three parts of the Stokes vector. The $A'_k(\theta_0)$ and $P'_k(\theta)$ are the two additional correction coefficients. For I , they are applied following the results of Zhu et al. (2022), which are depended on the view zenith angle (θ) and calculated based on Rayleigh scenes over sea surface. For polarimetric signals, the additional correction coefficients can be referred to Qie et al. (2021). The E_0 is the standard solar radiation flux and the $[I_N, Q_N, U_N]^T$ are the corrected normalized signals at top of the atmosphere of DPC.

In successful AOD retrieval, one of the key processes is to screen appropriate pixels. Cloud pixel is the main factor impacting aerosol retrieval, because they will block the signal from aerosol due to high reflectance, large coverage, and relatively high vertical position. Even very thin cirrus clouds and missed cloud edges can cause an ~~obviously~~ positive error of ~13% in visible channel



(Koren et al. 2007). To remove cloud pixels in DPC images, we used several universal methods by considering cloud-sensitive characteristics in radiative and polarized bands:

1) The first step is to filter the image with a 3×3 sliding window in blue (490 nm) and red (670 nm) bands for land and sea surfaces, respectively (Remer et al. 2012). If the standard deviation of a window is greater than 0.0025, then the center pixel will be marked as a cloud pixel and removed (Martins et al. 2002). This method was initially applied to the MODIS image by considering the spatial variability of aerosol and cloud pixels. In addition, a threshold of > 0.4 in the green (565 nm) band is also used to detect cloud pixels after the filter process, in accordance with the DT algorithm. This threshold is to exclude very uniformly distributed cloud pixels in the central area of thick clouds, and some snow pixels and glint area will also be excluded at the same time.

2) In second step, a whiteness test was applied by using reflectance in visible bands. It uses the characteristic that clouds are white in the visible band, considering that pixel with the absolute value of average relative deviations greater than 0.7 is cloud. In the absence of infrared and thermal infrared information, it can supplementally remove any pixels that have flat reflectance, similar to some operators using reflectance ratio to detect clouds. This method was proposed by Gomez-Chova et al. (2007) for Medium Resolution Imaging Spectrometer (MERIS) multispectral image, and it has also been considered in the well-known Fmask algorithm.

3) The third step used polarized bands to remove cloud pixels, following a fact that cloud drops can show a relatively strong polarized reflectance by multiple scattering (cloudbow effect) under a specify observation geometry. This feature has been used to generate cloud mask product for both POLDER and DPC sensors (Breon and Colzy 1999; Li et al. 2021). When the scattering angle (SCA) is between 127° and 157° , pixels with corrected polarized radiation at 865 nm larger than 0.03 and 0.05 for ocean and surface, respectively, are defined as cloud (Li et al. 2021). The relatively large SCA range is for a strict screening, given that the main peak of the polarized reflectance by cloud water droplets is $\sim 142^\circ$ (Goloub and Deuze 1994). In addition, any obvious noise is also removed in this step, such as the case of $\text{DOLP} > 1$.

3.3 Construction of Multi-pixel Retrieval Unit

Next, we will explain the necessary operations and settings of parameters to apply the GRASP algorithm to DPC data in detail. The GRASP algorithm can use the temporal and spatial continuity of pixels, and allow a group of pixels to be inverted at the same time. The multi-pixel retrieval unit for DPC in the study is shown as **Figure 1**. Each small cube represents a pixel in geographic grids with a spatial resolution of $0.1^\circ \times 0.1^\circ$ (3×3 DPC pixel averaged). This is in accordance with the MODIS 04_L2 product (~ 10 km). The projection is determined by the DPC data. Each pixel is guaranteed to have at least 3 different observation angles. Size of the retrieval unit can be arbitrarily selected, but limited by the hardware memory. Different colors show the percentage of land or sea, and usually do not change with time. They need to be clearly defined in GRASP to select different surface reflectance models. Cloud and no-data pixels need to be removed before the retrieval, because the cloud flag setting has not been implemented in the current version of code. Finally, this retrieval unit was applied in the GRASP to calculate the AOD distributions and compared with AERONET observations.

3.4 Settings of Retrieval Parameters

The settings of initial value and spatial-temporal constraint can significantly impact results of



the statistically optimized strategy in the GRASP algorithm (Dubovik et al. 2011). The GRASP allows different strategies to fit observations. ~~As the cases recorded in the GRASP software, there are two retrieval schemes.~~ The configurations of the two schemes are different only by settings of aerosol size distribution in the forward model. One fits the aerosol size distribution with 16 triangle bins from the range of 0.05 to 15.0 μm , while the other uses 5 lognormal bins at 0.1, 0.1732, 0.3, 1.0, and 2.9 μm , based on pre-calculated optimized kernels of the POLDER-3. The 5 lognormal bins scheme increases speed by ~ 9 times (2.5GHz CPU) without any graphical acceleration compared to the 16 triangle bins scheme, and it has been used to generate the operational PARASOL/GRASP aerosol products (Chen et al. 2020). In addition, there is a scheme that is being tested called “GRASP/Model”. This fits ~~observational signal~~ by externally mixing several aerosol types with fixed optical parameters, which is more stable and faster **to calculate** the AOD.

A tolerable absolute error in radiative transfer calculations is set to 0.0005 and the multiple scattering effects **has** been considered. **Number** of atmospheric layers is set to 10 with an exponential distribution. The input data of the GRASP algorithm was both normalized radiative measurements at 443, 490, 565, and 670 nm and DOLP of 490 and 670 nm. The initial guess of aerosol and surface properties are default in the GRASP software. They ~~comply with general principles and~~ are applied to calculate AOD at a global scale. The Ross-Li’s model (Li et al. 2001) and the Cox-Munk model (Cox and Munk 1954) were used for modeling radiative (non-polarized) reflectance over land and ocean, respectively, while, the surface polarized reflectance **was following** the method of Nadal and Bréon (1999). Among them, the complex refractive index and surface properties are generally allowed to be **fitted** as wavelength-dependent parameters in iterations. All constraints on values are given a default sizeable range, such as the first parameter in the Ross-Li’s model allowed to vary from 0.001 to 1.100. By light scattering calculations (Dubovik et al. 2006), all aerosol microphysical parameters are converted into optical parameters to participate in radiative simulation. Spatial and temporal constraints of variabilities of aerosol and surface properties are realized by using Lagrange multiplier method. More details can be referred to Dubovik et al. (2021). In this study, the GRASP/Model scheme was used to retrieve AOD from DPC. All calculations of the GRASP relied on the supercomputing system in the Supercomputing Center of Wuhan University.

4. Results and Discussions

4.1 Validation of DPC/GRASP with AERONET

As shown in **Figure 2**, the AERONET observations were used as the references to estimate the performance of AOD retrieval from DPC images based on the GRASP algorithm. Linear regression, correlation coefficient (R), Normalized Mean Square Error (NMSE), Mean Bias (MB), percentage falling into Expect Error (EE%), and matching Number (N) were also calculated. Overall, the DPC GRASP/Model AOD matches the AERONET observations with an R of 0.8590, a MB of 0.0189, and a NMSE of 0.1432. Nearly 80% of the GRASP/Model AOD retrievals fall within the expect error bounds, showing a good performance without any quality control. ~~While,~~ the slope of linear regression was 0.8438, ~~less than 1~~. This means that under heavy aerosol loading, the DPC/GRASP may underestimate the AOD. Although the additional radiometric correction factors were applied, negative drift due to DPC instrument attenuation probably reduces signals from strong reflectance and thus results lower values of AOD.



In order to further study the retrieval performance of GRASP/Model, control the quality of the retrieval result from DPC data, we calculated the dependences of NMSE with retrieval residuals, serial length and effective pixel number in retrieval units, and observation geometry, as shown in **Figure 3**. The retrieval absolute MB showed an obvious increase when the SCA is large than 150° . Critical observation conditions, such as pixels at the edge of the image, will probably result to a larger error in both satellite sensor and forward model. By contrast, different viewing angle number (3-11) have relatively little impact on the retrieval results, that the average absolute MB bias varies between 0.0395 and 0.0541. The same phenomenon was also found in the **Figure 3c**. With increase in length of retrieval units, the absolute MB was relatively stable, only fluctuating around 0.047. This indicated that the fitting scheme for using the external mixing of different aerosol types in this scheme of the GRASP/Model did not show much dependence of the length of the time series. By contrast, the absolute MB showed a decrease trend with the number of averaged pixels, from 0.082 to 0.041. It means that the GRASP/Model is relative sensitive to surrounding pixels in the study. In addition, the spatial-temporal constraints in the retrieval are also affected by Lagrange multipliers, which can be customized in the configuration file.

Fitting residual is an important factor to estimate the quality of retrieval in GRASP. It was found that the absolute MB showed a slight increase (from 0.047 to 0.063) when the radiative fitting residuals were larger than 8%. While, the absolute MB had a trend to decrease first and then increase, with increase in the polarized fitting residuals. Given that the DPC designed uncertainty is about 5% for radiometric measurements and 0.02 for DOLP, the relatively large absolute MB (0.069) at 0.01 of the polarized fitting residuals is caused by overfitting of GRASP/Model. To summarize, the SCA, number of averaged pixels, and fitting residuals showed the impacts on DPC GRASP/Model AOD retrieval in this test. Pixels with $SCA > 150$, number of averaged pixels < 4 , non-polarized fitting residual $< 8\%$, and $0.01 < \text{polarized fitting residual} < 0.08$, were removed as the low-quality retrievals.

Figure 4a showed the scatterplots and density distributions of DPC/GRASP AOD versus the AERONET observations after quality control. About a quarter of the points was removed. It was found that the performance of AOD retrieval from DPC images showed an enhancement. For DPC GRASP/Model, the R increased from 0.8590 to 0.8982, the EE% increased from 79.58% to 83.16%, the NMSE decreased from 0.1432 to 0.1008, and the MB decreased from 0.0189 to 0.0176. The slope of linear regression also showed a slight improvement with the value increasing from 0.8438 to 0.8867. **Figure 4b** displayed the relative frequency of differences between DPC and AERONET AOD. The peak values of deviation for DPC GRASP/Model were found at 0.0144, -0.0185, and -0.0935 when the $AOD < 0.2$, $0.2 \leq AOD < 0.5$, and $AOD \geq 0.5$, respectively. This shows that the MB drifts from positive to negative as AOD increases.

4.2 Evaluation of DPC AOD Performance at a Spatial Scale

The DPC AOD retrieved by the GRASP/Model was compared with AERONET observations at each individual site to show a world-wide retrieval result as **Figure 5**. The R, NMSE, MB, and EE% were calculated and displayed on sites where the matching number of pixels was larger than 10. In addition to the observation performance of the DPC itself, spatial variations in performances of AOD retrieval greatly depend on settings of initial parameter and constraint in the GRASP, whether they are in line with the local aerosol and surface environments. Results showed that the GRASP/Model achieved a great performance in different regions. The high values of R (> 0.8) were



found in most regions, while the several lower values (~ 0.6) were mainly observed in North America and South Africa. The NMSE showed the values of NMSE in most sites were less than 0.1. This means that $\sim 70\%$ values of AOD retrieval matched the true values very well. In several sites, such as western United States, the NMSE were larger than 2, revealing that the AOD has a relatively larger deviation calculated from DPC images based on current parameter setting with the GRASP algorithm in the regions. The values of AOD were overestimated (~ 0.05) in the most areas, as shown in MB of Figure 5c. By contrast, the underestimations were found in high aerosol loading regions, such as South Asia and North Africa, that MB values were between -0.02 and -0.06 , in accordance with the slope of linear regression of less than 1. The EE% showed that over 80% of AOD retrieved in sites can fall within the expect error. However, an abnormal relatively high EE% ($> 60\%$) from GRASP/Model was also found in the western United States where the NMSE was large and R was low. By compared with sites in central Africa, this phenomenon was probably due to the clean air and extremely low aerosol content there, and thus the NMSE showed relatively larger. It is worth noting that the parameterization in the GRASP/Model scheme is a globally consistent configuration in this study and does not consider the characteristics between different regions. This means that it is possible to achieve better results in local regions by adjusting different parameterizations.

To further estimate the performance of DPC/GRASP AOD, two regions were selected as cases as shown in Figure 6. The MODIS MAIAC, DT, and DB aerosol products were used as comparisons. It was noted that the DB algorithm was only executed over land in the C6.1 MODIS DB aerosol products. It was found that the spatial coverage of GRASP/Model AOD from DPC over land was slightly lower than the MAIAC MODIS aerosol products. In addition to the narrower field of view and longer re-visit cycle on DPC (MODIS operated in two satellite: Terra and Aqua), the cloud mask method probably also mis-classified the cloud-free pixels in heavy aerosol loading conditions. This also partially resulted the underestimation of DPC AOD because the heavy aerosol loading pixels are removed. Nevertheless, DPC still properly captures the spatial distribution of AOD. The highest AOD values (> 1.0) in the southern part of China (mainly Guangdong and Guangxi) were caught by the current retrieval strategy. This is in accordance with the three MODIS products. By contrast, the AOD found in North China Plain and Centre China by the DPC GRASP/Model (~ 0.5) were a little bit lower than MAIAC and DT products (~ 0.6). However, the DT aerosol products showed higher AOD in this region, closed to ~ 1.0 . This phenomenon owes to unsuitable aerosol models, which further results a persistent overestimation in DT algorithm (Che et al. 2019). By the additional radiometric and polarimetric correction, the DPC GRASP/Model showed good performance over both Land and Ocean. The high values of AOD in the South China Sea and the estuary of the Yangtze River can be clearly captured. To summarized, the DPC showed spatial ability of AOD retrieval based on GRASP algorithm in China region and the similar results have also been reported recently by using the GRASP/component module (Li et al. 2022).

Another case was selected in Western Europe where the air is clean and aerosol loading is low (< 0.2) in the most of time around year. As shown in Figure 6b, different satellites and aerosol retrieval methods showed slightly different distributions of AOD. In addition to the different transit times between DPC and MODIS, this phenomenon is also probably because the aerosol signal is difficult to separate from the total satellite observation under low aerosol loading conditions and thus result relative larger uncertainties of retrieval. From the AOD maps of DPC GRASP/Model, the relatively high values of AOD (~ 0.25) were found in Central France, Southern Spain, and Southern England. While, the MODIS MAIAC showed lower AOD (~ 0.1) over the mainland and



two points of high AOD (~ 0.5) were found in Northern coastal areas of Spain and Algeria. By contrast, the distributions of AOD calculated by DT and DB algorithm were also different from that calculated by DPC GRASP/Model and MAIAC. The high AOD (~ 0.4) region appeared in Northern France, Italy, and Southern England. Compared with single pixel-based retrieval algorithm (such as DT and DB), the GRASP and MAIAC considered more temporal and spatial information of aerosol and surface parameters. All of them have been proven to have good performance of AOD retrieval (Sayer et al. 2014; Lyapustin et al. 2018; Chen et al. 2020; Ou et al. 2021).

4.3 Comparison of DPC AOD with MODIS Products at a Temporal Scale

In this section, time-series of AOD were evaluated by compared with MODIS aerosol products based on the observations of AERONET site. The mean error ratios (MER) were calculated for the global collocation data set from 23 selected AERONET stations, as shown in **Figure 7**. The MER compares the mean bias for each satellite aerosol products in a specified period of time to their EE% (Gupta et al. 2018). Lower absolute value of MER means the smaller actual errors, indicating a good match with the AERONET. The selected AERONET stations had relatively continuous observations during the study period to avoid that global validation statistics shift in local emphasis and introduce temporal variation in the global results (Gupta et al. 2018). From the **Figure 7**, it was found that the time series of AOD from DPC GRASP/Model had a good matching with the AERONET AOD. The absolute values of MER were stable and less than ~ 0.05 after day 65. While the reason of relatively large negative MER (~ -0.1) before day 65 is presumed to be low EE%, as the DPC GRASP/Model would underestimate AOD under heavy aerosol loading conditions. This result is similar to the result of DT algorithm. Both showed good performances. In addition, the temporal averaged MER showed that the MODIS DT (0.0230) and DPC GRASP/Model (0.0049) generally overestimated the AOD, while the MODIS MAIAC (-0.0208) underestimated. By contrast, though the temporal averaged MER of MODIS DB was closer to 0, this was due to the cancellation between positive and negative biases. It is worth noting that the same parameter scheme (including start points and constraints) was applied globally in the GRASP/Model. Therefore, the difference in aerosol optical properties and spatial-temporal heterogeneity in different regions may be not considered appropriately. The optimization of the region is expected to improve the inversion effect.

Figure 8 showed three cases at different underlying surface to display the time series of AOD retrieved from DPC GRASP/Model on the basis of AERONET observations. The DT AOD was also compared as a reference, due to its stable performance. It was found that the behavior of AOD from DPC/GRASP and MODIS DT was generally consistent with AERONET at the three sites. From the scatterplots, the values of R were 0.983 and 0.928, 0.943 and 0.959, and 0.967 and 0.859 for MODIS DT and DPC GRASP/Model at Pilar_Cordob, Magurele_Inoe, and FZJ-JOYCE, respectively. The GRASP/Model AOD retrieved from DPC were slightly higher than the AERONET in the FZJ-JOYCE site and thus it resulted a relatively lower R. Nevertheless, in general, DPC/GRASP has a good ability to capture the temporal variation of aerosols.

Conclusion and Summary

The DPC/ GaoFen-5 is the first multi-angular polarized sensor launched by China and thus it has occupied an important position in the development of satellite sensors. In this study, AOD was retrieved from the DPC images by using the GRASP algorithm and compared with AERONET and



MODIS observations. The main purpose is to evaluate the performance of the DPC to monitor global aerosols.

On a global basis, a uniform parameterization scheme, which defined the variation ranges and start values of the optical and microphysical properties (realized by aerosol type) of the aerosol, was applied in the “Model” module of GRASP. Validations against AERONET showed that the R and EE% of DPC GRASP/Model were 0.8590 and 79.68%, respectively, in the first attempt. The SCA, number of averaged pixels in retrieval units, and fitting residual showed an impact on the results of AOD. A larger number of pixels in retrieval units and a smaller fitting residual can help improve the quality of retrieval. By quality control (SCA > 150, number of averaged pixels < 4, non-polarized fitting residual < 8%, and 0.01 < polarized fitting residual < 0.08 removed), the R and EE% of DPC GRASP/Model improve to 0.8982 and 83.16%, respectively. The corresponding MB and NMSE decreased from 0.0189 and 0.1432 to 0.0176 and 0.1008, respectively. This indicated that DPC has a good ability to detect aerosols under this scheme.

In the perspective of spatial scale, the R and EE% of GRASP/Model were larger than 0.9 and 80% respectively in the most AERONET sites. Large NMSE and Low EE were found in low aerosol loading conditions such as west of the United States. When the actual AOD is small, the retrieval bias of AOD from satellite observations will be amplified as reflected in NMSE and EE to some extent. By compared with MODIS aerosol products, the AOD from DPC GRASP/Model showed good consistency in China, that all regions with high AOD values were detected. Evaluation of the time-serial AOD showed the performance of DPC GRASP/Model is similar to the MODIS DT and better than MODIS DB and MAIAC products. Therefore, to summarize, the DPC can capture spatial and temporal variations in aerosols. The study improves to our understanding of DPC and find a solution for retrieving AOD based on GRASP algorithm. The continuous development of multi-angle sensors polarized plays an important role in aerosol monitoring in the future.

Acknowledgement

This study was funded by the National Key R&D Program of China (Grant No. 2018YFB0504500), National Natural Science Foundation of China (Grant No. 41875038, No. 42071348, and No. 42001291), the Key R&D projects in Hubei Province (Grant No. 2021BCA220) and supported by the LIESMARS Special Research Funding. We are grateful to the Moderate Resolution Imaging Spectroradiometer (MODIS) Team, the Aerosol Robotic Network (AERONET) Organization and the GaoFen-5 Directional Polarimetric Camera (DPC) Developed Team for freely distributed their aerosol products and measurements. The numerical calculations in this paper have been done on the supercomputing system in the Supercomputing Center of Wuhan University. Finally, we would also like to thank all reviewers for their constructive and valuable comments.

References

- Albrecht, B.A. (1989). AEROSOLS, CLOUD MICROPHYSICS, AND FRACTIONAL CLOUDINESS. *Science*, 245, 1227-1230
- Ångström, A. (1964). The Parameter of Atmospheric Turbidity. *Tellus*, 14
- Breon, F.M., & Colzy, S. (1999). Cloud detection from the spaceborne POLDER instrument and



- validation against surface synoptic observations. *Journal of Applied Meteorology*, 38, 777-785
- Breon, F.M., & Goloub, P. (1998). Cloud droplet effective radius from spaceborne polarization measurements. *Geophysical Research Letters*, 25, 1879-1882
- Che, H., Yang, L., Liu, C., Xia, X., Wang, Y., Wang, H., Wang, H., Lu, X., & Zhang, X. (2019). Long-term validation of MODIS C6 and C6.1 Dark Target aerosol products over China using CARSNET and AERONET. *Chemosphere*, 236, 124268
- Chen, C., Dubovik, O., Fuertes, D., Litvinov, P., Lapyonok, T., Lopatin, A., Ducos, F., Derimian, Y., Herman, M., Tanré, D., Remer, L.A., Lyapustin, A., Sayer, A.M., Levy, R.C., Hsu, N.C., Descloitres, J., Li, L., Torres, B., Karol, Y., Herrera, M., Herreras, M., Aspetsberger, M., Wanzenboeck, M., Bindreiter, L., Marth, D., Hangler, A., & Federspiel, C. (2020). Validation of GRASP algorithm product from POLDER/PARASOL data and assessment of multi-angular polarimetry potential for aerosol monitoring. *Earth System Science Data*, 12, 3573-3620
- Cox, C., & Munk, W. (1954). Measurement Of The Roughness Of The Sea Surface From Photographs Of The Suns Glitter. *Journal Of The Optical Society Of America*, 44, 838-850
- D'Almeida, G.A., Koepke, P., & Shettle, E.P. (1991). Atmospheric aerosols: Global climatology and radiative characteristics. *Journal of Medical Microbiology*, 54, 55-61
- Deschamps, P., Breon, F., Leroy, M., Podaire, A., Bricaud, A., Buriez, J., & Seze, G. (1994). The POLDER mission: instrument characteristics and scientific objectives. *Ieee Transactions on Geoscience and Remote Sensing*, 32, 598-615
- Deuzé, J.L., Bréon, F.M., Devaux, C., Goloub, P., Herman, M., Lafrance, B., Maignan, F., Marchand, A., Nadal, F., Perry, G., & Tanré, D. (2001). Remote sensing of aerosols over land surfaces from POLDER-ADEOS-1 polarized measurements. *Journal of Geophysical Research: Atmospheres*, 106, 4913-4926
- Diner, D.J., Beckert, J.C., Reilly, T.H., Bruegge, C.J., Conel, J.E., Kahn, R.A., Martonchik, J.V., Ackerman, T.P., Davies, R., Gerstl, S.A.W., Gordon, H.R., Muller, J.P., Myneni, R.B., Sellers, P.J., Pinty, B., & Verstraete, M.M. (1998). Multi-angle Imaging SpectroRadiometer (MISR) - Instrument description and experiment overview. *Ieee Transactions on Geoscience and Remote Sensing*, 36, 1072-1087
- Dubovik, Sinyuk, A., Lapyonok, T., Holben, B.N., Mishchenko, M., Yang, P., Eck, T.F., Volten, H., Munoz, O., & Veihelmann, B. (2006). Application of light scattering by spheroids for accounting for particle non-sphericity in remote sensing of desert dust. *Journal of Geophysical Research Atmospheres*, 111
- Dubovik, Fuertes, D., Litvinov, P., Lopatin, A., Lapyonok, T., Dubovik, I., Xu, F., Ducos, F., Chen, C., Torres, B., Derimian, Y., Li, L., Herreras-Giralda, M., Herrera, M., Karol, Y., Matar, C., Schuster, G.L., Espinosa, R., Puthukkudy, A., Li, Z., Fischer, J., Preusker, R., Cuesta, J., Kreuter, A., Cede, A., Aspetsberger, M., Marth, D., Bindreiter, L., Hangler, A., Lanzinger, V., Holter, C., & Federspiel, C. (2021). A Comprehensive Description of Multi-Term LSM for Applying Multiple a Priori Constraints in Problems of Atmospheric Remote Sensing: GRASP Algorithm, Concept, and Applications. *Frontiers in Remote Sensing*, 2
- Dubovik, O., Herman, Goldak, A., Lapyonok, T., Tanre, D., Deuze, J.L., Ducos, F., Sinyuk, A., & Lopatin, A. (2011). Statistically optimized inversion algorithm for enhanced retrieval of aerosol properties from spectral multi-angle polarimetric satellite observations. *Atmospheric Measurement Techniques*, 4, 975-1018
- Dubovik, O., & King, M.D. (2000). A flexible inversion algorithm for retrieval of aerosol optical properties from Sun and sky radiance measurements. *Journal of Geophysical Research Atmospheres*, 105, 20673-20696



- 499 Dubovik, O., Lapyonok, T., Litvinov, P., Herman, M., Fuertes, D., Ducos, F., Lopatin, A., Chaikovskiy,
 500 A., Torres, B., Derimian, Y., Huang, X., Aspörsberger, M., & Federspiel, C. (2014). GRASP: a versatile
 501 algorithm for characterizing the atmosphere. *SPIE Newsroom*
- 502 Eck, T.F., Holben, B.N., Reid, J.S., Dubovik, O., Smirnov, A., O'Neill, N.T., Slutsker, I., & Kinne, S.
 503 (1999). Wavelength dependence of the optical depth of biomass burning, urban, and desert dust aerosols.
 504 *Journal of Geophysical Research: Atmospheres*, 104, 31333-31349
- 505 Eck, T.F., Holben, B.N., Sinyuk, A., Pinker, R.T., Goloub, P., Chen, H., Chatenet, B., Li, Z., Singh, R.P.,
 506 Tripathi, S.N., Reid, J.S., Giles, D.M., Dubovik, O., O'Neill, N.T., Smirnov, A., Wang, P., & Xia, X.
 507 (2010). Climatological aspects of the optical properties of fine/coarse mode aerosol mixtures. *Journal of*
 508 *Geophysical Research*, 115
- 509 Gao, J., Woodward, A., Vardoulakis, S., Kovats, S., Wilkinson, P., Li, L., Xu, L., Li, J., Yang, J., Li, J.,
 510 Cao, L., Liu, X., Wu, H., & Liu, Q. (2017). Haze, public health and mitigation measures in China: A
 511 review of the current evidence for further policy response. *Science of the Total Environment*, 578, 148-
 512 157
- 513 Ge, B., Mei, X., Li, Z., Hou, W., Xie, Y., Zhang, Y., Xu, H., Li, K., & Wei, Y. (2020). An improved
 514 algorithm for retrieving high resolution fine-mode aerosol based on polarized satellite data: Application
 515 and validation for POLDER-3. *Remote Sensing of Environment*, 247
- 516 Goloub, P., & Deuze, J.L. (1994). Analysis of the POLDER polarization measurements performed over
 517 cloud covers. *IEEE Trans.geosci.remote Sens*, 32, 78-88
- 518 Gomez-Chova, L., Camps-Valls, G., Calpe-Maravilla, J., Guanter, L., & Moreno, J. (2007). Cloud-
 519 screening algorithm for ENVISAT/MERIS multispectral images. *Ieee Transactions on Geoscience and*
 520 *Remote Sensing*, 45, 4105-4118
- 521 Guo, J., Deng, M., Lee, S.S., Wang, F., Li, Z., Zhai, P., Liu, H., Lv, W., Yao, W., & Li, X. (2016). Delaying
 522 precipitation and lightning by air pollution over the Pearl River Delta. Part I: Observational analyses.
 523 *Journal of Geophysical Research: Atmospheres*, 121, 6472-6488
- 524 Gupta, P., Remer, L.A., Levy, R.C., & Mattoo, S. (2018). Validation of MODIS 3 km land aerosol optical
 525 depth from NASA's EOS Terra and Aqua missions. *Atmospheric Measurement Techniques*, 11, 3145-
 526 3159
- 527 Hagolle, O., Goloub, P., Deschamps, P.-Y., Cosnefroy, H., Briottet, X., Bailleul, T., Nicolas, J.-M., Parol,
 528 F., Lafrance, B., & Herman, M. (1999). Results of POLDER in-flight calibration. *Ieee Transactions on*
 529 *Geoscience and Remote Sensing*, 37, 1550-1566
- 530 Holben, B.N., Eck, T.F., Slutsker, I., Tanre, D., Buis, J.P., Setzer, A., Vermote, E., Reagan, J.A., Kaufman,
 531 Y.J., Nakajima, T., Lavenue, F., Jankowiak, I., & Smirnov, A. (1998). AERONET - A federated instrument
 532 network and data archive for aerosol characterization. *Remote Sensing of Environment*, 66, 1-16
- 533 Hsu, N.C., Jeong, M.J., Bettenhausen, C., Sayer, A.M., Hansell, R., Seftor, C.S., Huang, J., & Tsay, S.C.
 534 (2013). Enhanced Deep Blue aerosol retrieval algorithm: The second generation. *Journal of Geophysical*
 535 *Research: Atmospheres*, 118, 9296-9315
- 536 Hsu, N.C., Tsay, S.C., King, M.D., & Herman, J.R. (2004). Aerosol properties over bright-reflecting
 537 source regions. *IEEE Transactions on Geoscience & Remote Sensing*, 42, 557-569
- 538 Jin, S., Ma, Y., Zhang, M., Gong, W., Dubovik, O., Liu, B., Shi, Y., & Yang, C. (2019). Retrieval of 500
 539 m Aerosol Optical Depths from MODIS Measurements over Urban Surfaces under Heavy Aerosol
 540 Loading Conditions in Winter. *Remote Sensing*, 11, 2218
- 541 Jin, S., Zhang, M., Ma, Y., Gong, W., Chen, C., Yang, L., Hu, X., Liu, B., Chen, N., Du, B., & Shi, Y.
 542 (2021). Adapting the Dark Target Algorithm to Advanced MERSI Sensor on the FengYun-3-D Satellite:



- Retrieval and Validation of Aerosol Optical Depth Over Land. *Ieee Transactions on Geoscience and Remote Sensing*, 59, 8781-8797
- Kacenelenbogen, M., Leon, J.F., Chiapello, I., & Tanre, D. (2006). Characterization of aerosol pollution events in France using ground-based and POLDER-2 satellite data. *Atmospheric Chemistry and Physics*, 6, 4843-4849
- Kaufman, Y.J., Tanré, D., Gordon, H.R., Nakajima, T., Lenoble, J., Frouin, R., Grassl, H., Herman, B.M., King, M.D., & Teillet, P.M. (1997). Passive remote sensing of tropospheric aerosol and atmospheric correction for the aerosol effect. *Journal of Geophysical Research: Atmospheres*, 102, 16815-16830
- Koren, I., Remer, L.A., Kaufman, Y.J., Rudich, Y., & Martins, J.V. (2007). On the twilight zone between clouds and aerosols. *Geophysical Research Letters*, 34, 5
- Lenoble, J., Remer, L., & Tanre, D. (2013). *Aerosol Remote Sensing*. Springer-Verlag Berlin Heidelberg
- Levy, R.C., Mattoo, S., Munchak, L.A., Remer, L.A., Sayer, A.M., Patadia, F., & Hsu, N.C. (2013). The Collection 6 MODIS aerosol products over land and ocean. *Atmospheric Measurement Techniques*, 6, 2989-3034
- Li, J.H., Ma, J.J., Li, C., Wang, Y.Y., Li, Z.Q., & Hong, J. (2021). Multi-information collaborative cloud identification algorithm in Gaofen-5 Directional Polarimetric Camera imagery. *Journal of Quantitative Spectroscopy & Radiative Transfer*, 261
- Li, L., Che, H., Zhang, X., Chen, C., Chen, X., Gui, K., Liang, Y., Wang, F., Derimian, Y., Fuertes, D., Dubovik, O., Zheng, Y., Zhang, L., Guo, B., Wang, Y., & Zhang, X. (2022). A satellite-measured view of aerosol component content and optical property in a haze-polluted case over North China Plain. *Atmospheric Research*, 266, 105958
- Li, L., Dubovik, O., Derimian, Y., Schuster, G.L., Lapyonok, T., Litvinov, P., Ducos, F., Fuertes, D., Chen, C., Li, Z., Lopatin, A., Torres, B., & Che, H. (2019). Retrieval of aerosol components directly from satellite and ground-based measurements. *Atmospheric Chemistry and Physics*, 19, 13409-13443
- Li, X.W., Gao, F., Wang, J.D., & Strahler, A. (2001). A priori knowledge accumulation and its application to linear BRDF model inversion. *Journal of Geophysical Research-Atmospheres*, 106, 11925-11935
- Li, Z., Hou, W., Hong, J., Zheng, F., Luo, D., Wang, J., Gu, X., & Qiao, Y. (2018). Directional Polarimetric Camera (DPC): Monitoring aerosol spectral optical properties over land from satellite observation. *Journal of Quantitative Spectroscopy and Radiative Transfer*, 218, 21-37
- Li, Z.Q., Lau, W.K.M., Ramanathan, V., Wu, G., Ding, Y., Manoj, M.G., Liu, J., Qian, Y., Li, J., Zhou, T., Fan, J., Rosenfeld, D., Ming, Y., Wang, Y., Huang, J., Wang, B., Xu, X., Lee, S.S., Cribb, M., Zhang, F., Yang, X., Zhao, C., Takemura, T., Wang, K., Xia, X., Yin, Y., Zhang, H., Guo, J., Zhai, P.M., Sugimoto, N., Babu, S.S., & Brasseur, G.P. (2016). Aerosol and monsoon climate interactions over Asia. *Reviews of Geophysics*, 54, 866-929
- Lopatin, A., Dubovik, O., Fuertes, D., Stenchikov, G., Lapyonok, T., Veselovskii, I., Wienhold, F.G., Shevchenko, I., Hu, Q., & Parajuli, S. (2021). Synergy processing of diverse ground-based remote sensing and in situ data using the GRASP algorithm: applications to radiometer, lidar and radiosonde observations. *Atmos. Meas. Tech.*, 14, 2575-2614
- Lyapustin, A., Wang, Y., Korkin, S., & Dong, H. (2018). MODIS Collection 6 MAIAC algorithm. *Atmospheric Measurement Techniques*, 11, 5741-5765
- Ma, Y., Zhu, Y., Liu, B., Li, H., Jin, S., Zhang, Y., Fan, R., & Gong, W. (2021). Estimation of the vertical distribution of particle matter (PM_{2.5}) concentration and its transport flux from lidar measurements based on machine learning algorithms. *Atmospheric Chemistry and Physics*, 21, 17003-17016
- Martins, J.V., Tanré, D., Remer, L., Kaufman, Y., Mattoo, S., & Levy, R. (2002). MODIS Cloud screening



for remote sensing of aerosols over oceans using spatial variability. *Geophysical Research Letters*, 29
 McCormick, M.P., Hamill, P., Pepin, T.J., Chu, W.P., Swissler, T.J., & McMaster, L.R. (1979).
 SATELLITE STUDIES OF THE STRATOSPHERIC AEROSOL. *Bulletin of the American
 Meteorological Society*, 60, 1038-1046
 Mishchenko, M.I., & Travis, L.D. (1997). Satellite retrieval of aerosol properties over the ocean using
 polarization as well as intensity of reflected sunlight. *Journal of Geophysical Research: Atmospheres*,
 102, 16989-17013
 Nadal, F., & Bréon, F.M. (1999). Parameterization of Surface Polarized Reflectance Derived from
 POLDER Spaceborne Measurements. *IEEE Transactions on Geoscience & Remote Sensing*, 37, 1709-
 1718
 Nakajima, T., Yoon, S.C., Ramanathan, V., Shi, G.Y., Takemura, T., Higurashi, A., Takamura, T., Aoki,
 K., Sohn, B.J., Kim, S.W., Tsuruta, H., Sugimoto, N., Shimizu, A., Tanimoto, H., Sawa, Y., Lin, N.H.,
 Lee, C.T., Goto, D., & Schutgens, N. (2007). Overview of the Atmospheric Brown Cloud East Asian
 Regional Experiment 2005 and a study of the aerosol direct radiative forcing in east Asia. *Journal of
 Geophysical Research-Atmospheres*, 112, 23
 Ou, Y., Li, L., Ying, Z., Dubovik, O., Derimian, Y., Chen, C., Fuertes, D., Xie, Y., Lopatin, A., Ducos, F.,
 & Peng, Z. (2021). Spatio-Temporal Variability of Aerosol Components, Their Optical and
 Microphysical Properties over North China during Winter Haze in 2012, as Derived from
 POLDER/PARASOL Satellite Observations. *Remote Sensing*, 13, 2682
 Qie, L., Li, Z., Zhu, S., Xu, H., Xie, Y., Qiao, R., Hong, J., & Tu, B. (2021). In-flight radiometric and
 polarimetric calibration of the Directional Polarimetric Camera onboard the GaoFen-5 satellite over the
 ocean. *Appl Opt*, 60, 7186-7199
 Rao, C.R.N., Stowe, L.L., & McClain, E.P. (1989). REMOTE-SENSING OF AEROSOLS OVER THE
 OCEANS USING AVHRR DATA THEORY, PRACTICE AND APPLICATIONS. *International Journal
 of Remote Sensing*, 10, 743-749
 Remer, L.A., Mattoo, S., Levy, R.C., Heidinger, A., Pierce, R.B., & Chin, M. (2012). Retrieving aerosol
 in a cloudy environment: aerosol product availability as a function of spatial resolution. *Atmospheric
 Measurement Techniques*, 5, 1823-1840
 Rosenfeld, D., Lohmann, U., Raga, G.B., O'Dowd, C.D., Kulmala, M., Fuzzi, S., Reissell, A., & Andreae,
 M.O. (2008). Flood or drought: How do aerosols affect precipitation? *Science*, 321, 1309-1313
 Sayer, A.M., Hsu, N.C., Bettenhausen, C., & Jeong, M.J. (2013). Validation and uncertainty estimates
 for MODIS Collection 6 "Deep Blue" aerosol data. *Journal of Geophysical Research: Atmospheres*, 118,
 7864-7872
 Sayer, A.M., Munchak, L.A., Hsu, N.C., Levy, R.C., Bettenhausen, C., & Jeong, M.J. (2014). MODIS
 Collection 6 aerosol products: Comparison between Aqua's e-Deep Blue, Dark Target, and "merged" data
 sets, and usage recommendations. *Journal of Geophysical Research-Atmospheres*, 119, 13965-13989
 Shi, T., Han, G., Ma, X., Gong, W., Chen, W., Liu, J., Zhang, X., Pei, Z., Gou, H., & Bu, L. (2021).
 Quantifying CO₂ Uptakes Over Oceans Using LIDAR: A Tentative Experiment in Bohai Bay.
Geophysical Research Letters, 48, e2020GL091160
 Tanre, D., Breon, F.M., Deuze, J.L., Dubovik, O., Ducos, F., Francois, P., Goloub, P., Herman, M.,
 Lifermann, A., & Waquet, F. (2011). Remote sensing of aerosols by using polarized, directional and
 spectral measurements within the A-Train: the PARASOL mission. *Atmospheric Measurement
 Techniques*, 4, 1383-1395
 Tegen, I., & Lacis, A.A. (1996). Modeling of particle size distribution and its influence on the radiative



properties of mineral dust aerosol. *Journal of Geophysical Research Atmospheres*, 101, 19237-19244
 Zhang, M., Jin, S., Ma, Y., Fan, R., Wang, L., Gong, W., & Liu, B. (2021). Haze events at different levels
 in winters: A comprehensive study of meteorological factors, Aerosol characteristics and direct radiative
 forcing in megacities of north and central China. *Atmospheric Environment*, 245, 118056
 Zhdanova, E.Y., Chubarova, N.Y., & Lyapustin, A.I. (2020). Assessment of urban aerosol pollution over
 the Moscow megacity by the MAIAC aerosol product. *Atmospheric Measurement Techniques*, 13, 877-
 891
 Zhu, S., Li, Z., Qie, L., Xu, H., Ge, B., Xie, Y., Qiao, R., Xie, Y., Hong, J., Meng, B., Tu, B., & Chen, F.
 (2022). In-Flight Relative Radiometric Calibration of a Wide Field of View Directional Polarimetric
 Camera Based on the Rayleigh Scattering over Ocean. *Remote Sensing*, 14

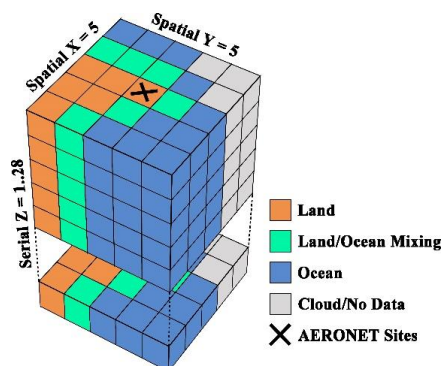


Figure 1. Schematic diagram for multi-pixel retrieval unit ($5 \times 5 \times 1..28$). A maximum of 28 sequences
 allowed in each unit is limited by hardware memory.

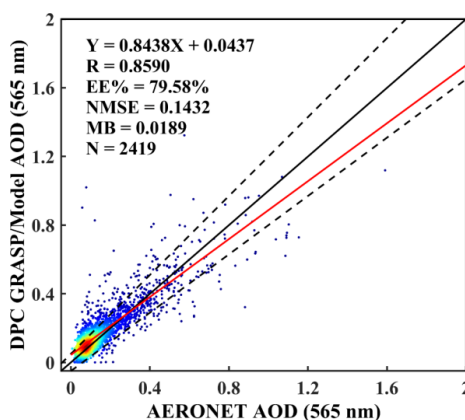


Figure 2. Two-dimensional density scatterplot of AOD retrieval from DPC with the GRASP/Model
 scheme versus the AERONET observations. The solid black lines are diagonal and the dashed black
 lines show the ranges of expect error. The red solid lines represent the linear regression lines.

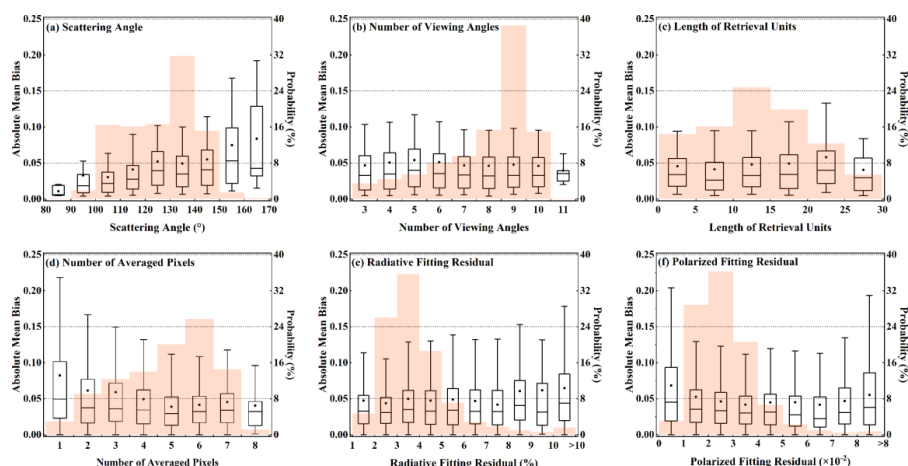


Figure 3. Influencing factors of AOD retrieval performance of DPC based on the GRASP/Model: (a) SCA; (b) number of viewing angles; (c) length of retrieval units; (d) number of averaged pixels; (e) non-polarized fitting residual; (f) polarized fitting residual. Orange shadows in the background represents the probability distribution of the samples.

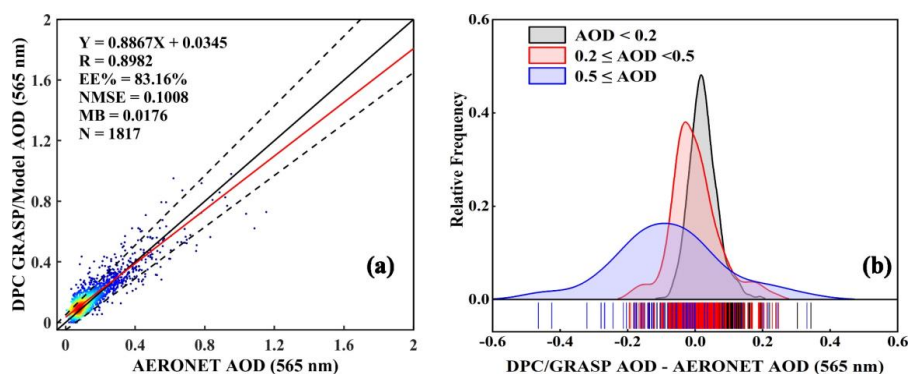


Figure 4. Performances of AOD retrieval from DPC data based on the GRASP/Model after quality control. (a) Two-dimensional density scatterplot of AOD retrieval from DPC with the GRASP algorithm versus the AERONET observations; (b) Relative Frequency of AOD differences between DPC/GRASP and AERONET.

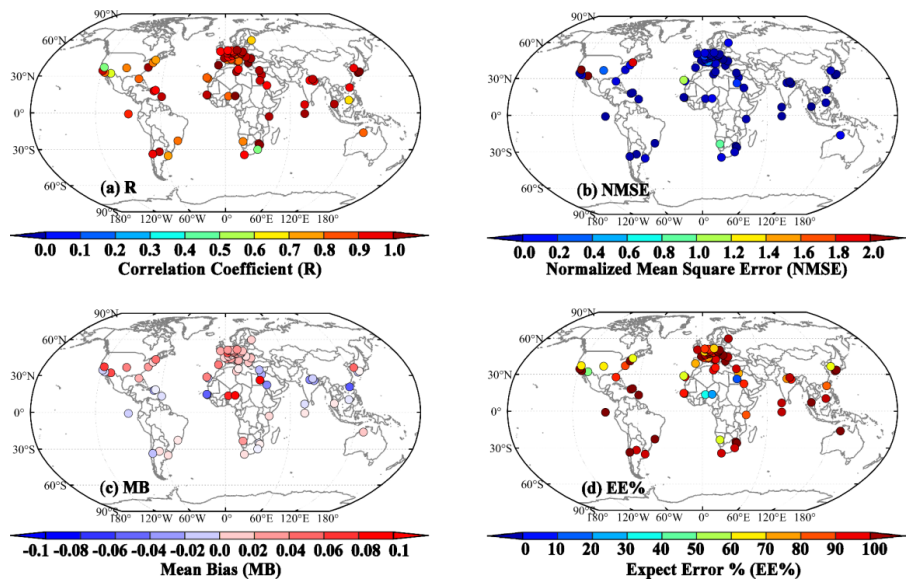


Figure 5. Spatial Distributions of (a) R, (b) NMSE, (c) MB, and (d) EE% calculated from DPC GRASP/model by compared with AERONET observations. Only sites with more than 10 matching points are included.

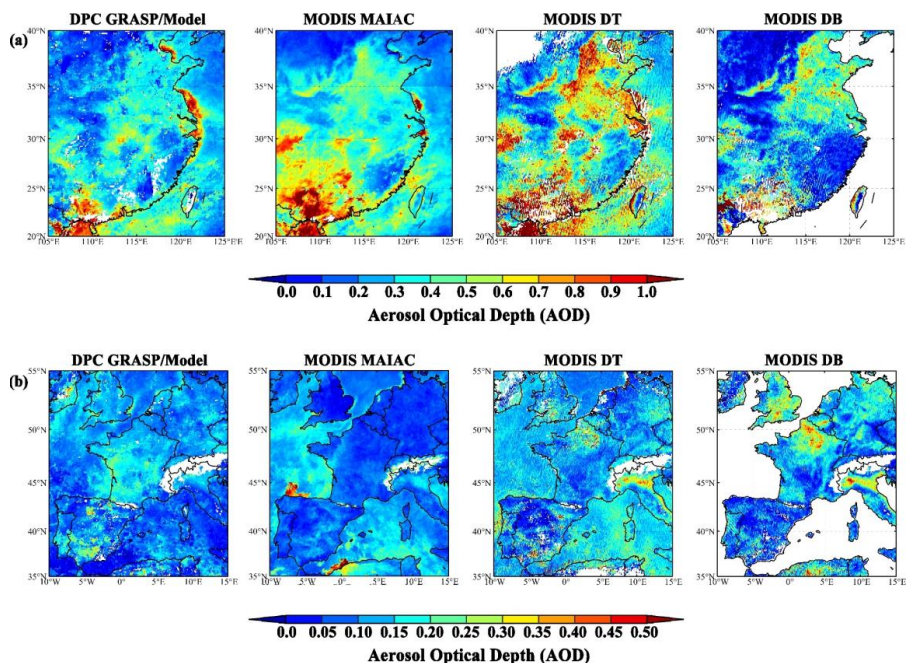


Figure 6. Spatial distribution of AOD from DPC GRASP/Model compared with MODIS MAIMC, DT, and DB aerosol products in March, 2020: (a) Eastern and Southern China with its adjacent sea areas. The dashed line is part of the Nine-dotted Line; (b) Areas of Western Europe including the



Atlantic Ocean and the Mediterranean. The DPC AOD is at 565 nm and the MODIS AOD is at 550 nm.

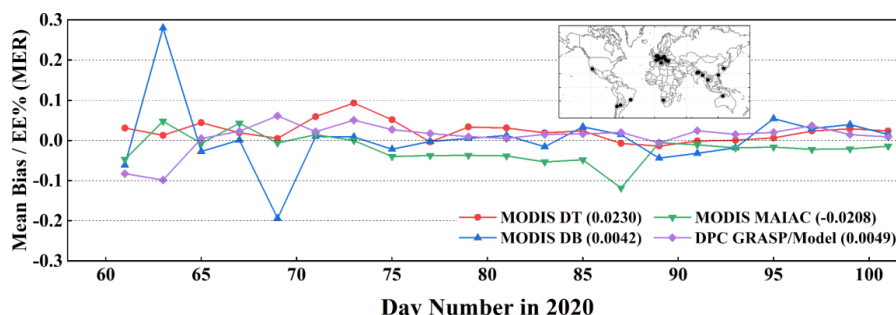


Figure 7. Time series of mean error ratios (MER) for the global collocation data set from 23 selected AERONET stations during March and April of 2020. The number in brackets are temporal averaged values of MER. The map inset shows the positions of AERONET stations with more details.

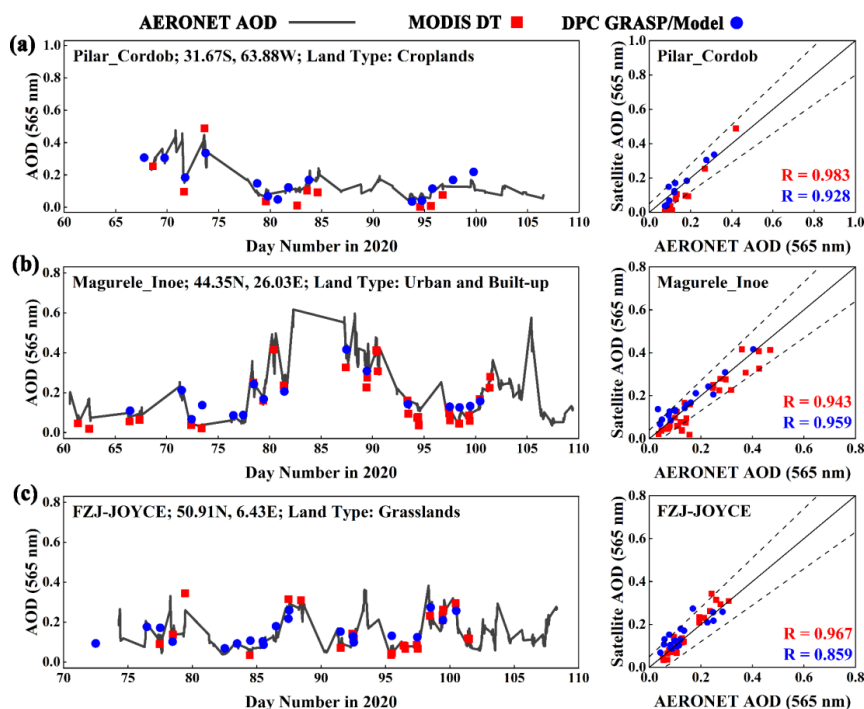


Figure 8. Time series of AOD from the DPC GRASP/Model versus the MODIS DT products and AERONET observations at three sites as cases: (a) Pilar_Cordob, (b) Magurele_Inoe, and (c) FZJ-JOYCE. The scatterplot shows the relationship between AERONET AOD and satellite AOD.